THE JOURNAL OF BIOLOGICAL CHEMISTRY VOL. 283, NO. 50, pp. 35173–35185, December 12, 2008

Human Wrnip1 Is Localized in Replication Factories in a Ubiquitin-binding Zinc Finger-dependent Manner*[S]

Received for publication, April 28, 2008, and in revised form, September 12, 2008 Published, JBC Papers in Press, October 7, 2008, DOI 10.1074/jbc.M803219200

Nicola Crosetto[‡1], Marzena Bienko[‡1,2], Richard G. Hibbert[§], Tina Perica[‡], Chiara Ambrogio[¶], Tobias Kensche[‡], Kay Hofmann[‖], Titia K. Sixma[§], and Ivan Dikic[‡3]

From the [‡]Institute of Biochemistry II and Cluster of Excellence "Macromolecular Complexes," "J. W. Goethe" University, Theodor-Stern-Kai 7, D-60590 Frankfurt (Main), Germany, [§]Molecular Carcinogenesis and Center for Biomedical Genetics, The Netherlands Cancer Institute, Plesmanlaan 121, 1066 CX Amsterdam, The Netherlands, [¶]Center for Experimental Research and Medical Studies and Department of Biomedical Sciences and Human Oncology, University of Torino, Via Santena 7, 10126 Torino, Italy, and [‖]Bioinformatics Group, Miltenyi Biotec GmbH, MACS Molecular Business Unit, 50829 Cologne, Germany

Wrnip1 (Werner helicase-interacting protein 1) has been implicated in the bypass of stalled replication forks in bakers' yeast. However, the function(s) of human Wrnip1 has remained elusive so far. Here we report that Wrnip1 is distributed inside heterogeneous structures detectable in nondamaged cells throughout the cell cycle. In an attempt to characterize these structures, we found that Wrnip1 resides in DNA replication factories. Upon treatments that stall replication forks, such as UVC light, the amount of chromatin-bound Wrnip1 and the number of foci significantly increase, further implicating Wrnip1 in DNA replication. Interestingly, the nuclear pattern of Wrnip1 appears to extend to a broader landscape, as it can be detected in promyelocytic leukemia nuclear bodies. The presence of Wrnip1 into these heterogeneous subnuclear structures requires its ubiquitin-binding zinc finger (UBZ) domain, which is able to interact with different ubiquitin (Ub) signals, including mono-Ub and chains linked via lysine 48 and 63. Moreover, the oligomerization of Wrnip1 mediated by its C terminus is also important for proper subnuclear localization. Our study is the first to reveal the composite and regulated topography of Wrnip1 in the human nucleus, highlighting its potential role in replication and other nuclear transactions.

Progression of DNA replication forks can be halted by DNA lesions or secondary structures, tight DNA-protein complexes, or the lack of deoxyribonucleotides (1). Several solutions have been selected throughout evolution to allow for the bypass of stalled replication forks and resume DNA synthesis. These include translesion synthesis, fork regression, and homologous recombination (1, 2). Failure in recovery of stalled replication forks may result in single and double strand DNA breaks, genomic instability, and if persistent, carcinogenesis (1).

Mgs1 (maintenance of genomic stability 1) was originally identified in bakers' yeast *Saccharomyces cerevisiae* as an evolutionarily conserved AAA^+ ATPase important for maintaining genomic stability (3). Subsequently, the mouse Mgs1 orthologue, Wrnip1 (Werner-interacting protein 1) was cloned as a binder of the helicase (Wrn) mutated in the Werner syndrome (4, 5). Telomere aberrations and defective telomere lagging-strand replication have been proposed to be a key patho-mechanism of this very rare premature aging condition, which remarkably recapitulates the main features of physiological aging (6, 7). In *S. cerevisiae*, *mgs1* was found to be synthetically lethal with the *rad6* and *rad18* genes involved in DNA damage tolerance, indicating that Mgs1/Wrnip1 might deal with stalled replication forks (8). A further study demonstrated that yeast Mgs1 can physically interact with the DNA loading clamp PCNA[4] and suggested that Mgs1 may participate in a DNA damage tolerance pathway alternative to the Rad6-Rad18 one (9). The inferred role of Mgs1/Wrnip1 in replication has been strengthened by the evidence that Mgs1 *in vitro* stimulates the activity of Fen1, an endonuclease indispensable for the removal of Okazaki fragments during lagging-strand replication (10). Additionally, purified human Wrnip1 can interact with DNA polymerase δ and increase the initiation efficiency of DNA replication *in vitro* (11). Besides a possible function in DNA replication, human Wrnip1 has also been shown to selectively bind ubiquitin (Ub) chains but not mono-Ub and has been proposed to regulate the turnover of ubiquitylated proteins (12). However, the precise function(s) of Wrnip1 in mammalian cells still remain unclear. It is conceivable that studies aimed at elucidating the function(s) of Wrnip1 in more detail may reveal unexpected insights in the mechanisms of DNA replication and their link to aging.

Here we show that in the nucleus of cultured cells human Wrnip1 is concentrated in a variety of structures, most of which

* This work was supported by Deutsche Forschungsgemeineschaft Grant DI 931/3-1 and grants from the Cluster of Excellence "Macromolecular Complexes" of the Frankfurt "J. W. Goethe" University (to I. D.) and NWO-CW (to T. S.). The costs of publication of this article were defrayed in part by the payment of page charges. This article must therefore be hereby marked "*advertisement*" in accordance with 18 U.S.C. Section 1734 solely to indicate this fact.

[S] The on-line version of this article (available at http://www.jbc.org) contains supplemental Figs. 1–3.

[1] Both authors equally contributed to this work.

[2] Recipient of the "J. Buchmann" scholarship.

[3] To whom correspondence should be addressed: Institute for Biochemistry II, Theodor-Stern-Kai 7, D-60590 Frankfurt am Main, Germany. E-mail: ivan.dikic@biochem2.de.

[4] The abbreviations used are: PCNA, proliferating cell nuclear antigen; Ub, ubiquitin; UBZ, ubiquitin-binding zinc finger; PML, promyelocytic leukemia; GST, glutathione *S*-transferase; DMEM, Dulbecco's modified Eagle's medium; PBS, phosphate-buffered saline; SPR, surface plasmon resonance; MALLS, multiangle laser light scattering; PIPES, 1,4-piperazinediethanesulfonic acid; RPA, replication protein A; UBA, ubiquitin-associated domain; Hs, Homo sapiens.

have a punctated, focal appearance and are visible throughout the cell cycle. A number of these foci overlap with replication factories, and the presence of Wrnip1 at DNA replication sites is greatly increased upon conditions that stall replication forks, such as UVC. Additionally, a proportion of Wrnip1 foci co-localize with promyelocytic leukemia (PML) bodies, independently of the cell cycle phase. Interestingly, the presence of Wrnip1 inside the aforementioned structures seems to specifically require its Ub-binding zinc finger domain (UBZ) as well as its ability to form oligomers. The presence of Wrnip1 at sites other than replication foci also hints at possible functions of this protein beyond DNA replication, which certainly deserve future attention.

EXPERIMENTAL PROCEDURES

Molecular Cloning—The following constructs were generated using the indicated restriction enzymes: pcDNA3.1-FLAG-Wrnip1 Mm and pGEX-Wrnip1 Hs (EcoRI and XhoI); pEGFP-N1-Wrnip1 Hs (EcoRI and BamHI); pGEX-UBZ^{Wrnip1} Hs (EcoRI and XhoI); pcDNA3.1-Myc-Rad18 Hs and pcDNA3.1-FLAG-Myc-Rad18 (EcoRI). pGEX-Ub and pGEX-Ub I44A have been described previously (13). Also pETM-30-UBZ^{Rad18} Hs has been described elsewhere (14). The cDNA used as a template in the generation of Wrnip1 constructs was obtained from the genomic consortium RZPD. The template for Rad18 constructs was HA-Rad18, which has been described previously (13). pBABE.puro-Wrnip1-EGFP was constructed by amplifying Wrnip1-EGFP from pEGFP-N1-Wrnip1 with primers containing the cleavage sequence of EcoRI. Substitution of Asp-37 to Ala in Wrnip1 and of Asp-221 to Ala in Rad18 was performed by PCR site-directed mutagenesis. The pBABE.puro-Wrnip1-EGFP and the pcDNA3.1-FLAG-Myc-Rad18 UBZ chimeras were obtained using the megaprimer mutagenesis method (15) and the sequence of *Mus musculus* polymerase ι, *Homo sapiens* polymerase η, and *H. sapiens* Wrnip1.

Antibodies and Other Chemicals—Anti-FLAG antibodies were from Sigma (M2 catalog number F3165 and M5 catalog number F4042), anti-PML (catalog number sc-966), anti-hemagglutinin (catalog number sc-7392), and anti-Myc (catalog number sc-40) antibodies from Santa Cruz Biotechnology, anti-Wrnip1 from GeneTex (catalog number GTX24731), and anti-EGFP from BD Biosciences (Living Colors® catalog number 632460).

Recombinant Proteins—The indicated GST fusions were obtained by inducing transformed *Escherichia coli* BL21 with 0.3 mM isopropyl 1-thio-β-D-galactopyranoside, when the culture reached A_{600} ≈1, and growing them overnight at 15 °C. Bacteria were then harvested in HEPES 20 mM, NaCl 150 mM, $ZnCl_2$ 2 μM, and β-mercaptoethanol 0.05%, supplemented with protease inhibitors just prior to use. The bacterial suspension was sonicated, and the lysate was cleared and then flown through a GSTrap™ HP column (GE Healthcare) mounted on an Äktaprime Plus chromatographic system (GE Healthcare). When indicated, GST was cleaved with thrombin (Amersham Biosciences).

Cell Culture, Transfection, and Synchronization—HEK 293T, Amphotropic Phoenix HEK 293, and HeLa cells were purchased from the American Tissue Culture Collection (ATCC) and grown in DMEM high glucose medium (Invitrogen), supplemented with penicillin (100 units/ml) and streptomycin (100 μg/ml) and 10% fetal bovine serum. After infection, HeLa cells were selected in the presence of 3 μg/ml puromycin.

HEK 293T were transfected using Lipofectamine reagent (Invitrogen) according to the manufacturer's instructions. HeLa and Phoenix Amphotropic 293 cells were transfected using Effectene (Qiagen).

For lysis, cells were incubated with a "Triton" buffer containing HEPES 50 mM, pH 7.5, NaCl 150 mM, EDTA 1 mM, EGTA 1 mM, Triton X-100 1%, glycerin 10%, NaF 25 mM, supplemented with protease inhibitors. The lysate was cleared, the supernatant collected (Triton X-100-soluble fraction), and the Triton-insoluble pellet resuspended in a buffer containing HEPES 50 mM, pH 7.4, NaCl 50 mM, $MgCl_2$ 2 mM, Triton X-100 0.1%, SDS 0.05%, and 2.5 units per μl of lysate of Benzonase® nuclease (Novagen). After 1 h of incubation at 4 °C, the suspension was centrifuged and the supernatant (Triton X-100-insoluble fraction) mixed with the Triton X-100-soluble fraction.

For synchronization, cells seeded on 10-cm Petri dishes containing one 12-mm coverslip per dish were grown to a confluency of 20–30%. At this point, thymidine was added to a final concentration 2 mM. After 18 h, cells were washed in PBS and put in fresh medium without thymidine. A second 17-h block was repeated 8 h after the first thymidine washout. At the time of the second release, a coverslip was taken for microscopy from one dish, whereas the remaining cells in the same dish were trypsinized and fixed in 70% ethanol. This procedure was repeated 5, 9, and 12 h after thymidine withdrawal. For cell cycle analysis, fixed cells were washed three times in PBS and resuspended in 2 ml of PBS containing 0.1% Triton X-100, 40 μg/ml propidium iodide (Sigma), and 100 μg/ml DNase-free RNase (Qiagen). After 30 min of incubation at 37 °C in the dark, the cell cycle distribution was analyzed using a Epics XL cytofluorimeter (Beckman Coulter) and the EXPO™32 ADC software (Beckman Coulter).

Virus Preparation and Infections—Retroviruses were produced by transfecting Amphotropic Phoenix HEK 293 cells with pBABE.puro constructs. Transfections were performed in 100-mm diameter dishes using Effectene (Qiagen), according to the manufacturer's instructions. Virus-containing supernatants were collected 24 and 48 h after transfection, cleared through a 0.2-μm pore diameter filter and supplemented with 8 μg/ml Polybrene (Sigma). 24 h after transfection, 5–10 × 10^4 target cells per well in a 6-well plate were infected with 500 μl of viral supernatant, and the medium was replaced after 8 h. The same procedure was repeated 48 h after transfection. 72 h after the first infection, selection of the infected cells was performed by adding puromycin to the growth medium.

Immune Precipitations and GST Pulldowns—Immune precipitations and pulldowns were done lysing a confluent well of a 6-well format plate with 500 μl of Triton buffer, and using 200 μl of lysate plus 200 μl of Triton buffer per reaction. After adding the indicated antibodies or GST fusions, the mixture was rotated for 4 h at 4 °C. In the case of immune precipitations, 20 μl of agarose-protein A were added per reaction 1 h before the end of rotation. Each sample was then washed four times

with 600 μl of Triton buffer. Agarose and Sepharose beads were resuspended in 25 μl of Laemmli buffer containing 5% β-mercaptoethanol and boiled for 5 min, and proteins were finally separated by SDS-PAGE.

Surface Plasmon Resonance (SPR)—Experiments were performed at 25 °C on a Biacore T-100 instrument (GE Healthcare). GST-UBZs or isolated UBZs were immobilized using an amine-coupling method to a CM5 chip at an immobilization density of 50–250 response units. Mono-Ub, Lys-48-, and Lys-63-type di-Ub chains were independently injected over the chip at concentrations of 128, 64, 32, 16, 8, 4, 2, and 1 μM, at 25 $\mu l \cdot min^{-1}$, with a 60-s association phase followed by a 5-min dissociation phase. A buffer consisting of 10 mM HEPES, pH 7.5, 150 mM NaCl, 2 μM $ZnCl_2$, 5 mM β-mercaptoethanol, and 0.05% Tween 20 was used throughout. Standard double referencing data subtraction methods were used before analysis of kinetics. Data analyses were performed using GraphPad Prism.

Size-exclusion Chromatography—Three confluent 10-cm dishes of HeLa_Wrnip1-EGFP cells were extracted as for laser scanning microscopy (see below) and lysed in 150 μl of a buffer containing HEPES 20 mM, pH 7.5, NaCl 50 mM, $ZnCl_2$ 2.5 μM, $MgCl_2$ 2 mM, dithiothreitol 1 mM, glycerin 10%, and Benzonase nuclease 4 μl/ml, supplemented with protease inhibitors. 4 mg of proteins were loaded onto a Superose 6 10/300 GL column (GE Healthcare) equilibrated with the same buffer used for cell lysis. Gel filtration was performed at 0.3 ml/min, and 100 fractions 0.2 ml each were collected.

Multiangle Laser Light Scattering (MALLS)—Static light scatterings experiments with MALLS were performed at 25 °C on a Mini-Dawn light scattering detector (Wyatt Technology) set online with a Superdex S75 10/30 column (GE Healthcare), in the same buffer used for SPR. Refractive index and light scattering detectors were calibrated against toluene and bovine serum albumin.

Induction of DNA Damage—For UVC treatment, cells on coverslips were washed once in PBS and UV-irradiated at 254 nm with a dose of 15 J/m^2. Afterward, fresh medium was added, and cells were incubated for 24 h before being processed for microscopy.

For hydroxyurea (Sigma) treatment, a stock solution of 100 mM in DMEM was added onto cells to a final concentration of 10 mM. Cells were then incubated for 24 h before extraction and processing for microscopy.

For topotecan (Hycamptin®, GlaxoSmithKline) treatment, cells grown on coverslips were placed in DMEM containing 1 μM topotecan for 3 h. Afterward, cells were washed with PBS and incubated in fresh medium for an additional 4 h before being processed for microscopy.

Laser Scanning Microscopy—Cells were grown on coverslips and transfected when indicated. For extraction with Triton X-100, cells were washed once in PBS and once in CSK buffer (10 mM PIPES, pH 6.8, 100 mM NaCl, 300 mM sucrose, 3 mM $MgCl_2$) and incubated for 3 min in CSK plus 0.3% Triton X-100. Cells were then washed three times with CSK, followed by one wash in PBS and fixed in 2% paraformaldehyde. Subsequently, cells were permeabilized for 10 min at room temperature, with a 0.2% Triton X-100 solution in PBS. All cells were blocked overnight at 4 °C in PBS containing 5% bovine serum albumin and 0.1% Tween 20. Primary and secondary antibodies were diluted in the blocking solution, and washes were performed in PBS plus 0.1% Tween 20. The coverslips were mounted on 10 μl of aqueous mounting medium (Biomeda) placed on a glass holder. Images were acquired by the LSM 510 META laser scanning microscope (Zeiss).

Quantifications of Microscopy Images and Statistical Analysis—To quantify the extent of co-localization between Wrnip1-EGFP and RPA, 44 Z-stacks composed on average of 6 slices were processed using the freely downloadable MacBiophotonics ImageJ software and the plugins "Colocalization Highlighter" and "Object Counter3D." To quantify the number of either Wrnip1- or Rad18-positive foci and their overlapping, 100 focal planes were analyzed using the LSM 510 META software on the expert mode. Details of the methods used to define intensity thresholds and foci are available upon request. To measure the amount of protein resistant to extraction by Triton X-100, 200 focal planes were examined for each experimental condition. Each nucleus was selected, and the mean intensity of pixels per nucleus together with the standard deviation (S.D.) were read. Comparisons were done using a Student's *t* likelihood test, considering the two distributions normal and their variances dissimilar.

Yeast Two-hybrid System—The yeast strain Y190 was transformed as described previously (16) with empty pYTH9 or pYTH9-Wrnip1 as a bait, and pACT2-Wrnip1, pACT2-Wrnip1 D37A, or Wrnip1 fragments in pACT2 prey. Yeasts were grown on a synthetic dropout (SD) medium without leucine and tryptophan (SD/−Trp/−Leu). Colonies appearing after 3 days on the selection medium were grown overnight in 5 ml of liquid selection medium. 0.5 ml of overnight culture were grown in 4.5 ml of SD/−Trp/−Leu medium for 1–2 h, and the concentration of cells was estimated by measuring the A_{600}, and the amount of cells per ml was adjusted by diluting with fresh medium. 5 μl of cell suspension containing the same amount of cells were spotted on SD/−Trp/−Leu agar plates as well as on 3′AT agar plates. The 2nd day after spotting, cells were transferred to a Whatman filter paper and assayed for β-galactosidase activity with 5-bromo-4-chloro-3-indolyl-β-D-galactopyranoside (X-gal; Roth).

RESULTS

Wrnip1 Can Interact with Both Mono- and Poly-ubiquitin—We have recently described two Ub-binding domains, UBM and UBZ, in the Y-family of translesion DNA polymerases. UBM and UBZ recognize ubiquitylated PCNA and are important for translesion synthesis (13). Following that discovery, we have pursued a computational prediction of proteins bearing either UBM or UBZ domains and grouped the latter into eight groups (13). Among all proteins predicted to contain one or more UBZ domains, those having a known or putative function in DNA damage responses carried either a type 3 or type 4 UBZ module (Fig. 1*A*). Compared with the UBZ of polymerase η, which belongs to the UBZ3 class, a major difference in the UBZ4 group was the fourth zinc ligand residue, which is a Cys instead of His as in UBZ3. Other more subtle differences between these two UBZ classes were also found. For instance, the invariant Asp residue within the second zinc-

binding dyad of UBZ3-type domains could also be found in many UBZ4 fingers but was not as well conserved within the UBZ4 family. The same trend held true for several other residues (indicated by *asterisks* in Fig. 1*A*), which have been recently proposed to be involved in binding to Ub (17). In contrast, the region around the first zinc-binding dyad appeared to be better conserved in UBZ4 as compared with UBZ3 (Fig. 1*A*).

We focused our attention on Wrnip1/Mgs1, which was recently shown to selectively bind poly-Ub chains and regulate the turnover of ubiquitylated proteins (12). Wrnip1 has been genetically linked to the ubiquitin ligase Rad18 in yeast and chicken cells and proposed to function in response to stalling of DNA replication forks (8, 18, 19). Because Rad18 is known to accumulate in a UBZ-dependent manner at sites of DNA damage (20), and because Wrnip1 UBZ is very similar to the one in Rad18 (Fig. 1*A*), we wondered whether the zinc finger domain of Wrnip1 may regulate its subnuclear distribution. We reasoned that by studying this phenomenon we may cast light on what appears to be a general UBD requirement for proteins containing them to form foci (13, 21–24).

First, we wanted to confirm that Wrnip1 can bind to Ub and that its UBZ is necessary and sufficient for such interaction. It has been recently shown that Wrnip1 can bind to poly- but not mono-ubiquitin (12). To validate these findings, we fused the amino acids 9–48 spanning the UBZ domain of human Wrnip1 in-frame with GST, expressed such fusion in *E. coli,* and used it to pull down a mixture of Ub chains varying in length from 2 to 7 monomers, linked either via lysine 48 or 63. Indeed, the UBZ domain of Wrnip1 could bind to both types of chains (data not shown). However, when overexpressed in HEK 293T cells, Wrnip1 could also interact with mono-ubiquitin either fused in-frame with GST and bound to glutathione-Sepharose or coupled to agarose beads (Fig. 1*B*). In contrast, Wrnip1 did not bind to the GST-fused Ub mutant I44A (Fig. 1*B*). This residue lies in the so-called "hydrophobic" patch on the surface of ubiquitin, and it is crucial for the interaction of Ub with the majority of known

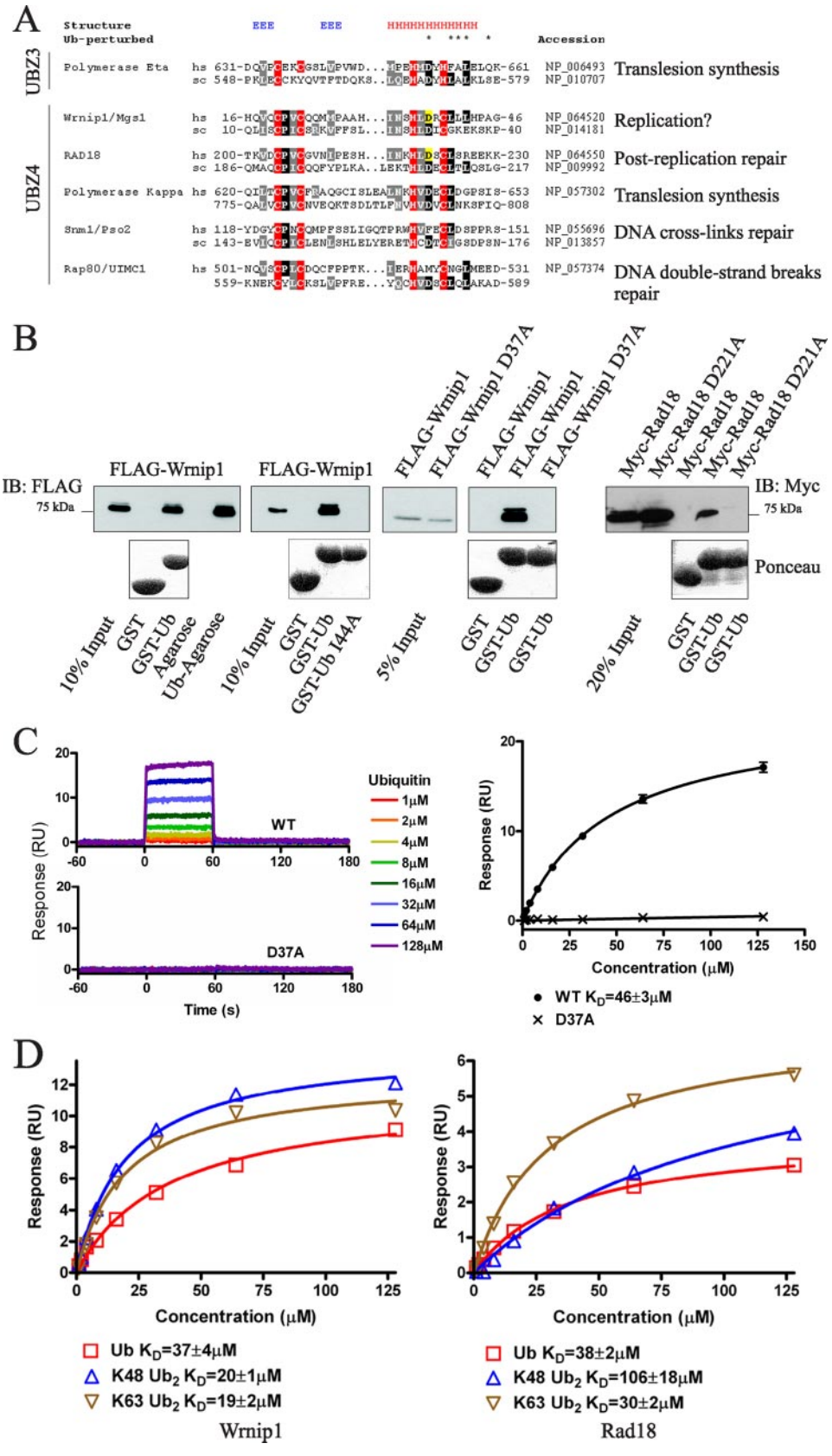

UBDs (25, 26). In agreement with previous findings (12), we also found that mutation to alanine of the highly conserved aspartate residue at position 37 in the human and mouse sequences of Wrnip1 (D37A) abolishes binding to both mono- and poly-Ub. This mutant corresponds to the previously described D652A mutant of polymerase η (13), which does not disrupt the overall structure of the zinc finger, being placed in the outer surface of the adjacent α-helix involved in direct interaction with Ub (17). When overexpressed in HEK 293T cells, the Wrnip1 D37A mutant could not be pulled down by GST-Ub, unlike wild-type Wrnip1 (Fig. 1*B*). Similarly, when the corresponding aspartate residue at position 221 in Rad18 was mutated to alanine, its interaction with mono-Ub was abolished (Fig. 1*B*).

To gain further insight in the binding properties of Wrnip1 UBZ, we fused it in-frame with GST and used the purified fusion protein for SPR with a Biacore flow system. As shown in Fig. 1*C*, clear binding curves could be seen for the wild-type protein, with a dissociation constant for the complex between wild-type GST-UBZ^{Wrnip1} bound to the chip and free mono-Ub estimated to be 46 μM from the equilibrium responses. The binding displayed fast-on fast-off kinetics, as expected for a low affinity interaction. In the case of the D37A mutant, no significant binding was seen with Ub concentrations up to 128 μM, confirming a dissociation constant for ubiquitin far in excess of this value. To exclude that the GST moiety affects the interaction between UBZ and Ub, we cleaved it by thrombin and coupled the purified UBZ domain to the chip for SPR (Fig. 1*D*). Similarly, we obtained a K_D of ~40 μM in the case of wild-type Wrnip1 UBZ bound to mono-Ub (Fig. 1*D*). As a control, we used the purified UBZ of Rad18 and obtained a K_D of 38 μM, consistent with the previously published value of 42 μM for GST-UBZ^{Rad18} (14). These data demonstrate that Wrnip1 and Rad18 UBZs can bind mono-Ub with comparable affinities, not surprising given their high sequence similarity. However, we observed a difference when di-Ub chains linked either via lysine 48 or 63 were flown over the UBZs of Wrnip1 and Rad18. In the case of Wrnip1, K_D values for both Lys-48- and Lys-63-type Ub_2 chains were slightly reduced, indicating a stronger interaction, whereas in the case of Rad18 this was observed only for Lys-63 chains. In contrast, the K_D value of Rad18 for Lys-48-linked di-ubiquitin was around 100 μM (Fig. 1*D*). These results demonstrate that Wrnip1 and Rad18 UBZs can bind both mono- and distinct poly-Ub chains and highlight a difference in chain-type selectivity between the two domains, despite their sequence similarity.

Wrnip1 Is Concentrated in Replication Factories and Other Subnuclear Structures—To gain knowledge on the biological function of human Wrnip1, we decided to examine its nuclear distribution by laser scanning microscopy. Among several tested antibodies, only one managed to detect Wrnip1 in fixed cells. Typically, Wrnip1 was confined in the nucleus, where it was mostly diffuse and excluded from nucleoli (data not shown). To visualize potential Wrnip1-positive subnuclear structures, we pretreated the samples with a mild detergent solution. This procedure has been largely applied to a variety of other nuclear proteins, unmasking distribution patterns otherwise shaded by their nucleoplasmic fraction (see for example Refs. 27, 28). Indeed, after extraction with Triton X-100, most of the diffuse Wrnip1 signal disappeared, and the remaining portion was predominantly detectable as discrete foci visible in all cells (Fig. 2*A*). Such focal structures were typically spread all over the nuclear sections examined, rarely found in nucleoli, and appeared round and isolated. Interestingly, in female HeLa cells, but not in MRC5 male fibroblasts, Wrnip1 was also spread in large patches (Fig. 2*A*), reminiscent of chromosomal territories (29). The antibody used seems rather specific in native conditions, as it detected only one prominent endogenous Wrnip1 band in immune precipitation (supplemental Fig. 1*A*).

To enhance the detection sensitivity and better visualize Wrnip1 structures, we established HeLa cells stably expressing low amounts of EGFP-tagged human Wrnip1 (HeLa_Wrnip1-EGFP). As expected, Wrnip1-EGFP was exclusively localized in the nucleus (Fig. 2*A*), and its average expression was comparable with that of endogenous Wrnip1 in the same cells and in the parental HeLa cell line (supplemental Fig 1*B*). The localization of Wrnip1-EGFP fully mirrored that of endogenous Wrnip1, with focal structures and patches that completely overlapped with endogenous Wrnip1 (Fig. 2*A*). Moreover, Wrnip1-EGFP and endogenous Wrnip1 co-fractionated in high molecular weight complexes (supplemental Fig. 1*C*), further indicating that the recombinant protein can recapitulate the behavior of endogenous Wrnip1. In the same fractionation experiment, Wrnip1 and Wrnip1-EGFP were also found to co-fractionate with PCNA and polymerase η, both of which have been previously shown to be in complex with Wrnip1 (9, 30).

Because Wrnip1 has been linked to replication, possibly operating in the bypass of stalled replication forks (3, 8, 9, 11, 18), we became interested in verifying whether any of the focal structures visualized in human cells contain replication factories. For this purpose, we stained HeLa_Wrnip1-EGFP cells with antibodies recognizing specific replication factors. In cells

FIGURE 1. **Wrnip1 is a mono- and poly-Ub-binding protein.** *A,* Wrnip1 contains a UBZ4 domain. Multiple alignment of UBZ3 (*upper part*) and UBZ4 (*lower part*) zinc finger domains is shown. Invariant or conserved in at least 40% of the sequences residues are shown on a *black* or *gray background*, respectively. The *two uppermost lines* indicate the secondary structure (E = extended, H = helix) of polymerase η and the residues (*asterisks*) with NMR signals that were perturbed upon Ub binding (17). The beginning and the end of each domain are indicated by the number of their first and last amino acids, respectively. Accession numbers are shown for each protein and refer to the NCBI Protein data base. Known or proposed functions of each protein are indicated on the *right*. *B,* Wrnip1 UBZ is necessary for interaction with mono-Ub. *Left panel,* GST-Ub and Ub-agarose pulldown of mouse FLAG-Wrnip1 overexpressed in HEK 293T cells. *2nd panel* from the *left,* GST-Ub I44A pulldown of *M. musculus* (*Mm*) FLAG-Wrnip1 overexpressed in HEK 293T. *2nd panel* from the *right,* GST-Ub pulldown of *M. musculus* FLAG-Wrnip1 D37A overexpressed in HEK 293T. *Right panel,* pulldown of Myc-tagged human Rad18 wild-type and D221A with GST-Ub. *IB,* immunoblot. *C,* Wrnip1 UBZ is a mono-Ub-interacting domain. *Left graphs,* sensorgrams obtained for different concentrations of free mono-Ub flown over wild-type (*upper left graph*) and D37A (*lower left graph*) GST-UBZ^{Wrnip1}. K_D values were calculated by fitting a Langmuir binding isotherm to the data (*right graph*). *D,* Wrnip1 and Rad18 UBZs have a different selectivity for di-ubiquitin chains. Isolated UBZs of Wrnip1 (*left graph*) and Rad18 (*right graph*) were coupled to a chip for SPR, and responses to increasing concentrations of either mono-Ub, Lys-48-, or Lys-63-linked di-ubiquitin chains were measured. The equilibrium responses obtained were plotted against Ub concentration, and K_D values were calculated from these Langmuir binding isotherms.

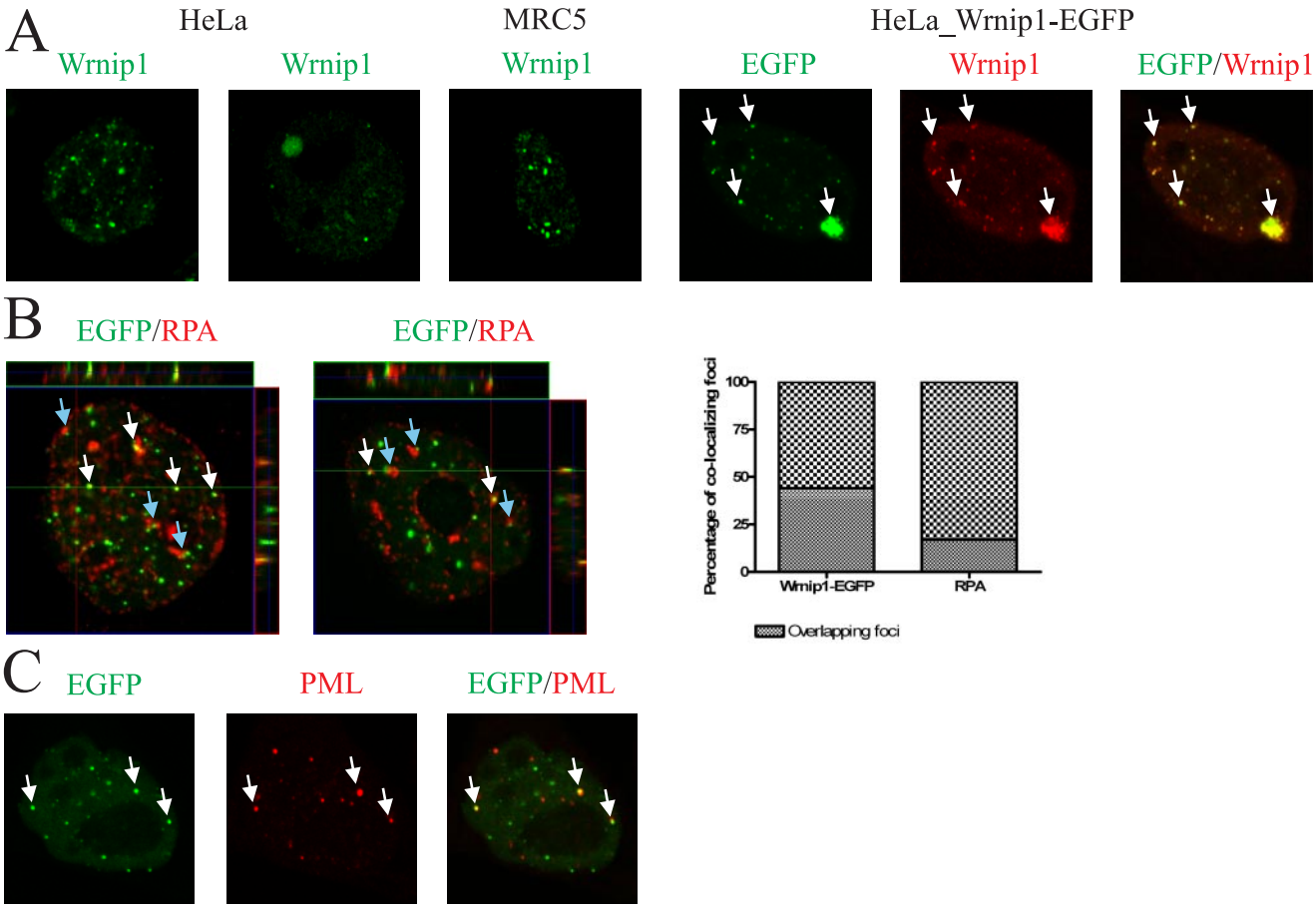

FIGURE 2. **Wrnip1 is concentrated in various subnuclear structures.** *A,* Wrnip1 is localized in punctated and patch-like structures in the absence of induced DNA damage. Endogenous Wrnip1 in HeLa and MRC5 cells (*left panels*). Endogenous and recombinant Wrnip1 fully co-localize in HeLa cells stably expressing low levels of Wrnip1-EGFP (*right panels*). Wrnip1-EGFP was detected using the fluorescence signal from EGFP, whereas endogenous Wrnip1 was probed with a commercially available anti-Wrnip1 antibody. *B,* some Wrnip1 foci correspond to replication factories. HeLa_Wrnip1-EGFP cells were stained with an antibody against RPA. Wrnip1-EGFP was detected using the fluorescence signal from EGFP. *Rectangles* on the *top* and *right side* of each squared image represent signal profiles along the *z* axis. *Histograms* on the *right,* quantification of the percentage of Wrnip1-EGFP foci overlapping with RPA and of RPA foci co-localizing with Wrnip1. *C,* some Wrnip1 foci overlap with PML bodies. HeLa_Wrnip1-EGFP cells were stained with an antibody against PML. In all the images, *white arrows* indicate examples of co-localizing proteins and *blue arrows* abutting foci.

recognizable as being in S phase by the presence of RPA foci, 44% of Wrnip1-EGFP-positive foci on average fully co-localized with replication factories, and 17% of replication foci contained Wrnip1 (Fig. 2*B*). In the same cells, we also observed many Wrnip1 foci partially overlapping with or abutting to replication foci (Fig. 2*B*, *blue arrows*). Similar results were obtained after visualization of replication factories with an antibody against PCNA (supplemental Fig. 2*A*).

The identity of Wrnip1 foci in non-S phase cells and of foci not overlapping with replication factories still remained obscure. To cast light on this intriguing issue, we undertook an hypothesis-driven approach and first tested for Wrnip1 co-localization with two subnuclear domains reminiscent in size and morphology of Wrnip1 foci: Cajal bodies and PML bodies. Cajal bodies are marked by coilin and have been functionally linked to small nuclear RNA biogenesis, telomerase RNA maturation, and transcription (31). No overlap between Wrnip1 foci and Cajal bodies was detected (data not shown). In contrast, in asynchronous HeLa_Wrnip1-EGFP cells, three Wrnip1 foci on average stained positive for PML per focal plane (Fig. 2*C*). A similar trend was seen between endogenous Wrnip1 and PML in the parental HeLa strain (supplemental Fig. 2*B*). Altogether, these data reveal a composite nuclear topography for Wrnip1 and demonstrate that Wrnip1-EGFP can recapitulate the behavior of endogenous Wrnip1 by localizing to physiological structures such as replication factories and PML bodies.

Wrnip1 Foci Are Dynamic during the Cell Cycle and after Replication Fork Stalling—Because in asynchronized cell cultures Wrnip1 foci of heterogeneous size can be appraised in various numbers in all nuclei (data not shown), we asked whether Wrnip1 is expressed in all the phases of the cell cycle. For this purpose, we synchronized HeLa cells with a double thymidine block and monitored the expression of endogenous Wrnip1 by Western blot. Comparable amounts of Wrnip1 protein could be detected in all the phases (Fig. 3*A*). We next wondered if the distribution of Wrnip1 foci changes throughout the cell cycle. Using the same procedure, we synchronized HeLa_Wrnip1-EGFP cells and fixed them at various time points after releasing the thymidine block. Wrnip1 foci were clearly present in all the four phases of the cell cycle, within most of the nuclei examined. During S phase, Wrnip1 foci were quite abundant, round, and relatively small (Fig. 3*A*, 0 h after thymidine withdrawal). This is consistent with the co-localization pattern between Wrnip1 and replication factors as

described before (Fig. 2*B*). When cells reached late S/early G_2 phase, the pattern changed, and Wrnip1 foci often appeared in linear or circular groups (Fig. 3*A*, 5 h after thymidine withdrawal). Many round-shaped Wrnip1 foci were again visible during mitosis and in early G_1 (Fig. 3*A*, 9 h after thymidine withdrawal and *small panels boxed* in *red*). Interestingly, a Wrnip1 signal could be also detected at the cleavage furrow (Fig. 3*A*, *white arrows* in the *red boxed panels*), which has been recently shown to be enriched in ubiquitylated proteins (32). Finally, when most of the cells were synchronized at the boundary between G_1 and S phase, the number of Wrnip1 foci dropped, and they appeared larger (Fig. 3*A*, 12 h after thymidine withdrawal). These data indicate that, besides being detected in large numbers during S phase, when many of them overlap with replication factories, Wrnip1 foci are also present in all the other phases of the cell cycle. This observation supports the idea that Wrnip1 could play extra-replicative functions.

We then wondered if and how agents known to stall replication forks affect the number and/or morphology of Wrnip1 foci. For this purpose, we treated HeLa_Wrnip1-EGFP cells with UVC light, hydroxyurea, or the topoisomerase I inhibitor topotecan and monitored their influence on Wrnip1 localization. In all cases, but particularly after UVC, the amount of Wrnip1-positive foci increased, and they tended to become confluent (Fig. 3*B*). When we quantified the mean number of foci per focal plane, a significant difference emerged between unstimulated and UVC-irradiated cells (Fig. 3*B*). We also observed that, upon UVC, the amount of Triton X-100-resistant Wrnip1 became significantly higher ($p < 0.001$) as compared with untreated cells, whereas the overall Wrnip1 protein levels remained constant (Fig. 3*B*). Altogether, these data demonstrate that Wrnip1 foci respond to conditions that block progression of replication forks by undergoing a dramatic re-organization in number, morphology, and solubility.

Type 4 UBZ of Wrnip1 Is Essential for Foci Formation—We have previously reported that the UBM and UBZ domains of Y polymerases are required for their presence inside nuclear foci representing replication factories (13, 21). Similarly, the integrity of Rad18 zinc finger is essential for its accumulation at sites of DNA damage (20). Because we also detected Wrnip1 foci both in nontreated cells (Fig. 2*A*) and upon replication forks stalling (Fig. 3*B*), we sought to verify whether this distribution requires its UBZ domain.

For this purpose, we examined by laser scanning microscopy HeLa cells stably expressing either wild-type EGFP-tagged Wrnip1 or its Ub-binding-deficient D37A mutant. After pretreating the coverslips with Triton X-100, no foci could be detected in cells expressing the D37A mutant, independently of UVC treatment (Fig. 4*A*, *left panels*). The same result was obtained after overexpression in HeLa cells of an EGFP-tagged Wrnip1 lacking the UBZ domain (Fig. 4*A*, *left panels*). In agreement with previous reports (20, 33), Rad18 similarly required its Ub-binding ability to be seen inside foci in UVC-treated cells (Fig. 4*A*, *right panels*). Additionally, we are the first to report that the same behavior applies to Rad18 in untreated cells (Fig. 4*A*, *right panels*).

Because Wrnip1 and Rad18 share a very similar UBZ4 domain (Fig. 1*A*), we wondered whether this would be sufficient to target these two proteins to the same set of foci. In HeLa_Wrnip1-EGFP cells transfected with Myc-Rad18, a relatively small fraction of Wrnip1- and Rad18-positive foci overlapped (Fig. 4*B*, *left panels* and *graph*). After treating cells with UVC light, the extent of co-localization significantly increased ($p < 0.001$), but it never reached a complete overlap in all cells (Fig. 4*B*, *right panels* and *graph*). These data demonstrate that Wrnip1 and Rad18 co-segregate in a subset of nuclear foci, possibly based on binding of their UBZs to the same ubiquitylated targets. However, they also reveal that very similar UBZ domains are not sufficient to drive full co-localization of UBZ-containing proteins into the same foci.

To further clarify these issues, we constructed Wrnip1 chimeras in which the UBZ domain was substituted by either the N-terminal UBM domain of polymerase ι, the type 3 UBZ domain of polymerase η, or the type 4 UBZ of Rad18. In addition, we made a Myc-tagged Rad18 chimera by exchanging the UBZ domain with the one of Wrnip1. We assume that such chimeras were properly folded because they all retained several properties of Wrnip1, such as nuclear localization and the ability to bind ubiquitin (supplemental Fig. 3*A*). Nevertheless, only Wrnip1 UBZ^{Rad18} and Myc-Rad18 UBZ^{Wrnip1} chimeras were detectable inside nuclear foci like the wild-type counterparts (Fig. 4*C*). In contrast, all the other chimeras showed a spread distribution (Fig. 4*C*) similar to that of Wrnip1 D37A (Fig. 4*A*). Our data indicate that the presence of Wrnip1 and Rad18 inside focal structures specifically depends on their type 4 UBZ domains, rather than on mere Ub binding ability. We hypothesize that the specific amino acid sequence and/or conformation of Wrnip1 and Rad18 Ubiquitin-binding domains are necessary for them to contact an unknown "attractor" inside nuclear foci.

Wrnip1 Oligomerization via Its C Terminus Contributes to Foci Localization—It has been shown previously that Wrnip1 forms homo-oligomers (11) and that its Ub-binding zinc finger may be involved in this process (34). Similarly, it has been demonstrated that Rad18 can dimerize (35) and that its UBZ domain is indispensable for this phenomenon (36). However, in contrast with these findings, the UBZ domain in Rad18 has been recently disproved to form oligomers *in vitro* (14). Therefore, it remains unclear whether type 4 Ub-binding zinc fingers can mediate oligomerization, which in turn could be required for proper localization. To clarify this issue, we first checked whether Wrnip1 D37A, which does not bind to Ub (Fig. 1, *B* and *C*), could still interact with wild-type Wrnip1 *in vivo*. In a yeast two-hybrid assay, Wrnip1 interacted with both Wrnip1 wild-type as well as with the D37A mutant (Fig. 5*A*). Equally, an interaction was detected between Wrnip1 wild type and a fragment encompassing the residues 397–665 of Wrnip1, but not with fragments containing either the residues 1–250 (including the UBZ domain) or 200–400 that contain the ATPase domain (Fig. 5*A*). In agreement with these findings, the previously described Wrnip1 $UBM^{Polι}$ chimera was still able to co-immunoprecipitate with wild-type Wrnip1 (Fig. 5*B*), further indicating that Wrnip1 UBZ is not important for homo-oligomerization.

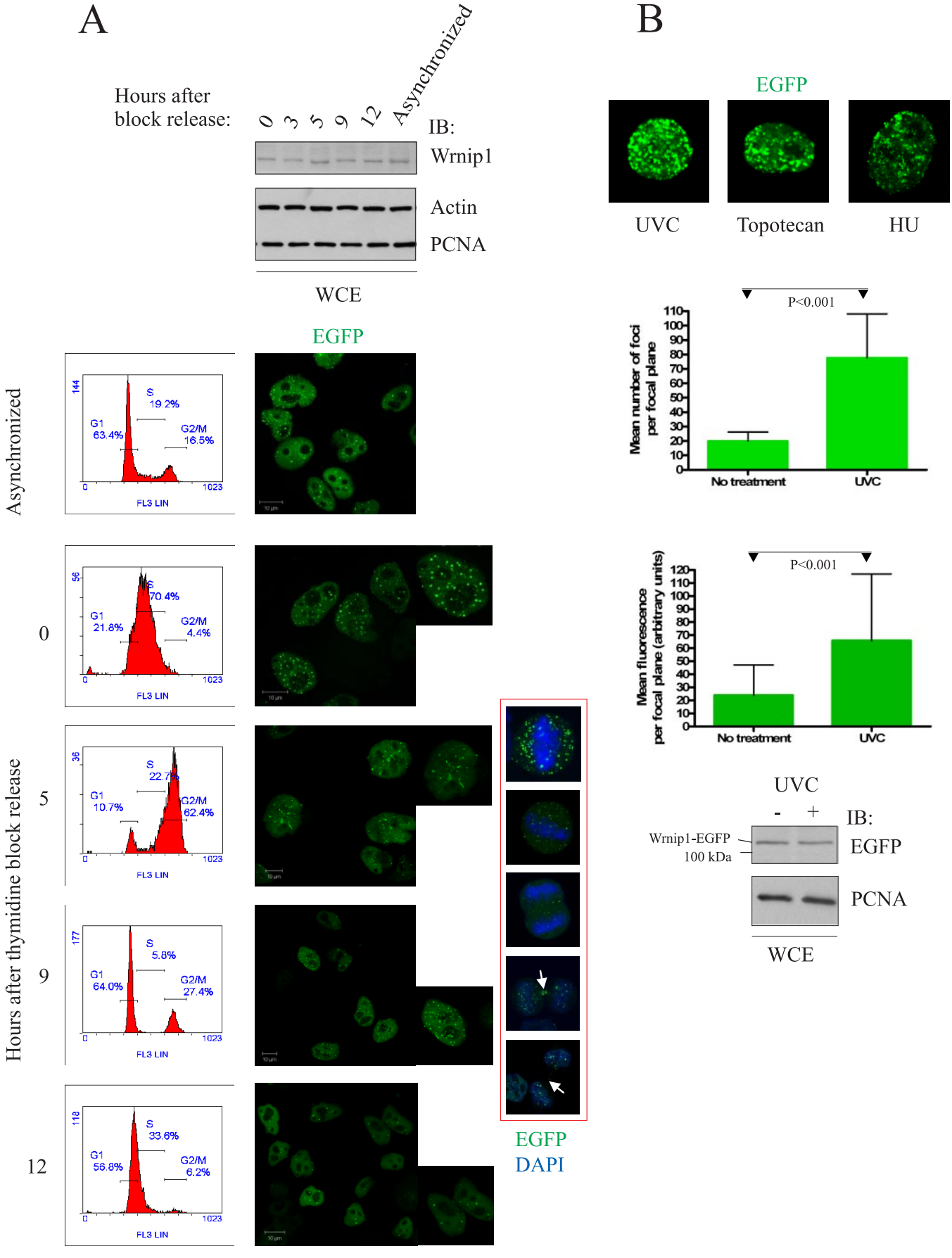

To conclusively exclude a role of Wrnip1 UBZ in oligomerization, we checked whether purified UBZ^{Wrnip1} expressed in *E. coli* is present in solution as either a monomer or an oligomer. Using MALLS, we measured a mass of 5.8 kDa for the amino acid sequence 9–48 of human Wrnip1, which encompasses the UBZ domain (Fig. 5*C*). This value is consistent with a monomeric UBZ domain, which has a molecular mass of 4.9 kDa. Furthermore, the mass estimated from the scattered light did not vary across the UBZ peak while being eluted from the size-exclusion chromatographic column, proving that the sample was monodisperse even at high concentrations (Fig. 5*C*). Altogether, our data indicate that the UBZ domain of Wrnip1 is not involved in oligomerization. On the contrary, the C-terminal portion of Wrnip1 seems relevant for this process.

Finally, we asked whether Wrnip1 oligomerization is important for its presence inside nuclear foci. For this purpose, we constructed various FLAG-tagged Wrnip1 fragments lacking progressively longer amino acid stretches from the C terminus. In HEK 2393T cells, all the fragments were expressed at higher levels than wild-type FLAG-Wrnip1 and bound to mono-Ub (supplemental Fig. 3*B* and data not shown). Only the fragment containing amino acids from 1 to 450 (encompassing the UBZ and the AAA^+ domain, but lacking the predicted leucine zipper at position 496–547 (34)) retained appreciable ability to bind Wrnip1, although deficient in comparison with the wild-type protein (supplemental Fig. 3*B*). In contrast, the fragment 1–380 was almost unable to bind GST-Wrnip1. In HeLa_Wrnip1-EGFP cells, the fragment 1–450 was not distributed inside foci but completely diffuse inside the nucleus (Fig. 5*D*). The same pattern was observed in the case of all other fragments (data not shown). In contrast, full-length FLAG-Wrnip1 was enriched within focal structures that also contained Wrnip1-EGFP (Fig. 5*D*). In conclusion, these data confirm our finding that the C-terminal third of Wrnip1 is required for oligomerization (Fig. 5*A*). Additionally, they reveal that already the last 215 amino acids of Wrnip1, which appear to contribute to oligomerization (supplemental Fig. 3*B*), are critical for Wrnip1 presence in nuclear foci.

DISCUSSION

In all organisms, recovery of stalled DNA replication forks is critical to maintain genomic stability and can occur through multiple mechanisms and factors (1). In *S. cerevisiae*, Mgs1 (maintenance of genomic stability 1) is required to ensure genomic stability (3) and is likely to operate in a DNA damage-tolerance pathway alternative to Rad6-Rad18 (8, 9). In mammals, the orthologue of Mgs1, Wrnip1, was cloned as a binder of the helicase (Wrn) that is missing in the premature aging Werner syndrome (37) and functions in various DNA transactions, including replication (4). Human Wrnip1 has been shown to interact with DNA polymerase δ and inferred to operate in the re-start of stalled replication forks (11). However, the exact function(s) and regulation of Wrnip1 in human cells remain to be elucidated.

In this study, we provide a comprehensive structure-function analysis of Wrnip1 in human cells and show that Wrnip1 is distributed in a composite set of subnuclear structures. Unraveling the identity of these structures may cast light on the myriad of potential Wrnip1 functions in the cell. Besides a diffuse fraction, a part of Wrnip1 in the nucleus is mainly concentrated in a mix of punctated focal structures (Fig. 2*A*). Despite having been cloned as a Werner syndrome helicase (Wrn) binder, the distribution of Wrnip1 in undamaged cells does not mirror the one of Wrn. In line with several other reports (38–40), by light microscopy we were able to detect Wrn inside nucleoli but not in punctated structures.[5] Wrnip1 foci can be clearly seen throughout the cell cycle, but prominently during the S phase (Fig. 3*A*). At this time, many Wrnip1 foci overlap with replication factories marked either by the RPA and PCNA (Fig. 2*B* and supplemental Fig. 2*A*) or by Rad18 (Fig. 4*B*). This observation strengthens the evidence accumulated so far that Wrnip1 functions at DNA replication forks and can interact with certain replication factors, such as PCNA, polymerase δ, and FEN1 (9–11). Additionally, a dramatic re-organization of Wrnip1 topography is seen in the nucleus after treatment with UVC, topotecan, or hydroxyurea; the amount of detergent-resistant and plausibly chromatin-bound Wrnip1 significantly increases, as does the number of foci (Fig. 3*B*). Also, the percentage of Wrnip1 foci co-localizing with replication forks significantly increases (Fig. 4*B*), suggesting that human Wrnip1 may deal with stalled replication forks, as inferred previously from yeast studies (3, 8, 9).

The distribution of Wrnip1 in the nucleus, however, is not a mere reflection of the one of replication sites. Wrnip1 foci are visible in all the phases of the cell cycle, possibly representing various functional pools of this protein. In an effort to unravel the identity of these structures, we found that Wrnip1 is always present in a subset of PML bodies (Fig. 2*C*), independently of the cell cycle phase. PML bodies have been linked to a plethora of functions, including regulation of transcription, stress responses, alternative lengthening of telomeres, and establishment of heterochromatin after replication (41). Whether PML bodies represent a storage or an active site for Wrnip1 and whether, like PML, Wrnip1 is involved in heterochromatin formation are exciting topics for future investigations.

[5] N. Crosetto, M. Bienko, and I. Dikic, unpublished observations.

FIGURE 3. **Wrnip1 foci are dynamic.** *A,* Wrnip1 foci are visible throughout the cell cycle. HeLa_Wrnip1-EGFP cells were synchronized by a double thymidine block. *Top,* the overall amount of endogenous Wrnip1 remains constant throughout the cell cycle. *WCE*, whole cell extract. *Left column panels,* cell cycle phase distributions assessed by propidium iodide stain and cytofluorimetry. *Right column panels,* low magnification fields of asynchronized or synchronized HeLa cells. The *small panels* show representative magnifications of one or two cells found in the bigger adjacent panels. The *five small panels boxed* in *red* display nuclei in subsequent phases of mitosis. *White arrows* mark Wrnip1 signal at the cleavage furrow. Wrnip1-EGFP was detected using EGFP fluorescence. *IB*, immunoblot. *DAPI*, 4′,6-diamidino-2-phenylindole. *B,* Wrnip1 is re-distributed following DNA damage. *Top,* HeLa_Wrnip1-EGFP cells were treated with the indicated DNA-damaging agents, extracted, fixed, and used for microscopy. In the *middle,* quantification of the images above. Each *green histogram* represents mean values, whereas *black bars* mark standard deviations. *P,* result of a Student's *t* test comparing the indicated distributions. *Bottom,* the overall amount of Wrnip1 does not change upon UVC treatment. *WCE*, whole cell extract; *IB*, immunoblot; *HU*, hydroxyurea.

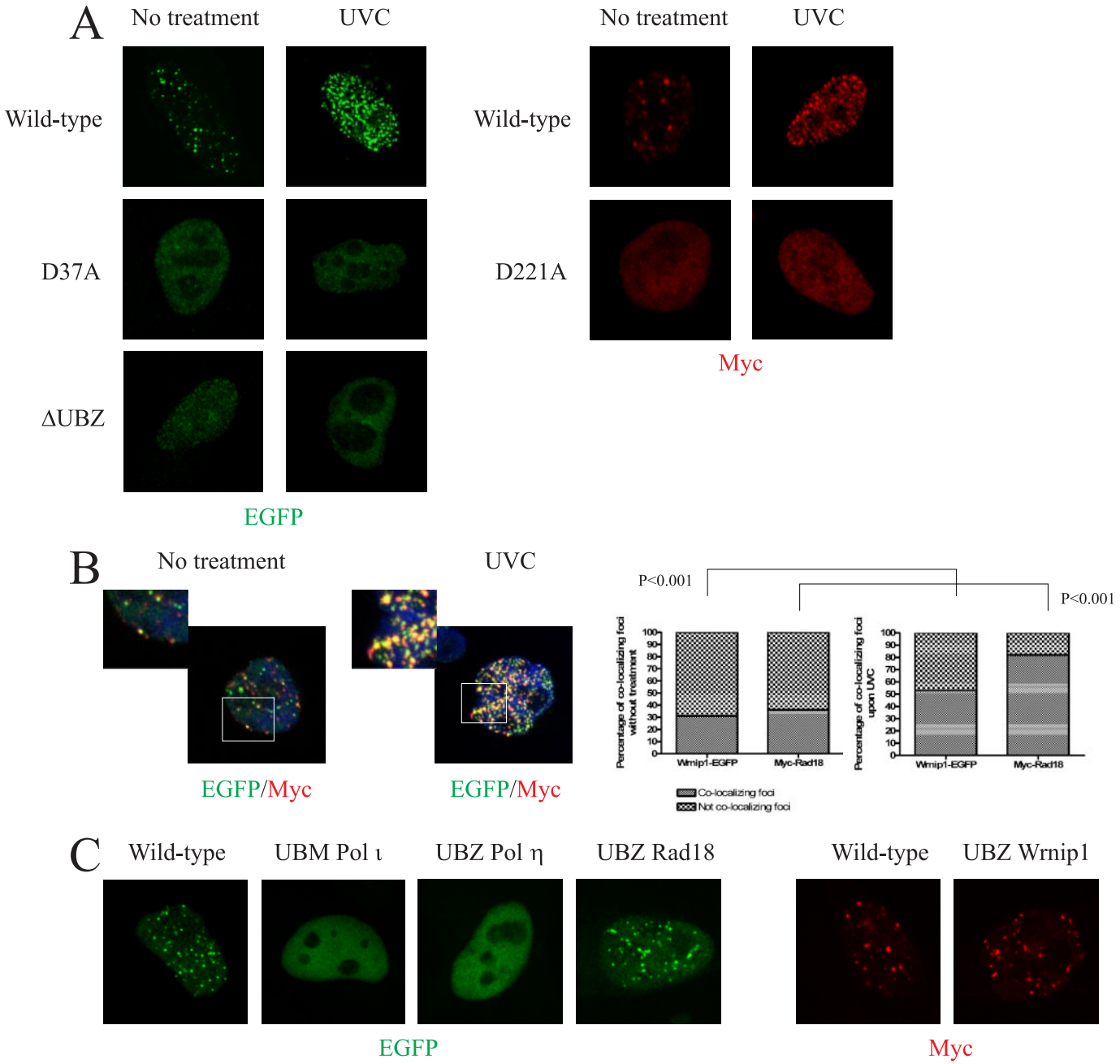

FIGURE 4. **Wrnip1 UBZ is essential for its localization to nuclear foci.** *A,* Wrnip1 and Rad18 UBZ are indispensable for their presence in nuclear foci, independently of DNA damage. *Left panels,* HeLa_Wrnip1-EGFP either wild-type or D37A as well as HeLa cells transfected with Wrnip1 ΔUBZ-EGFP were extracted, fixed, and used for microscopy. *Right panels,* HeLa_Wrnip1-EGFP cells transfected with either wild-type or D221A human Myc-tagged Rad18 were similarly processed. Wrnip1-EGFP was detected using EGFP fluorescence, Myc-Rad18 using an anti-Myc antibody. *B,* Wrnip1 and Rad18 co-localization is significantly enhanced by UVC irradiation. HeLa_Wrnip1-EGFP cells were transfected with Myc-tagged Rad18 and either treated with UVC irradiation (*right*) or not (*left*). The *white square* encloses the area that is magnified in the small panels. Wrnip1-EGFP was detected using the fluorescence from EGFP, whereas Myc-Rad18 using anti-Myc antibodies. *Histograms* on the *right,* quantification of Wrnip1-positive foci containing also Rad18 and of Rad18-positive foci containing Wrnip1, with or without prior UVC irradiation. The distributions were compared by a Student's *t* test, and the calculated *p* values are displayed. *C,* type 4 UBZ is required for Wrnip1 and Rad18 to be localized in foci. *Left,* HeLa cells transfected with Wrnip1-EGFP wild-type and various UBZ chimeras. *Right,* HeLa cells transfected with Myc-Rad18 wild-type and UBZ^{Wrnip1} chimera. Wrnip1-EGFP was detected using EGFP fluorescence, Myc-Rad18 using an anti-Myc antibody.

Such a composite topography is not limited to Wrnip1, because a similar pattern is observed in the case of certain DNA damage-responsive factors outside the S phase and in the absence of induced DNA damage. For example, the DNA damage tolerance ubiquitin ligase Rad18 is present in punctated structures in all the nuclei of asynchronized cells (20).[5] Approximately 15% of these foci also contain Wrnip1 (Fig. 4*B*). Wrnip1 foci in non-S phase cells might represent inactive depots or sites of extra-replicative functions, such as DNA damage repair or chromatin remodeling. Supporting the latter hypothesis, it is worth mentioning that Wrnip1 is an AAA^+ ATPase (3), with similarities to the protein chaperone and extractor Cdc48/p97. Like Wrnip1, Cdc48/p97 is a Ub-binding protein and an AAA^+ ATPase able to extract protein complexes involved in a multi-

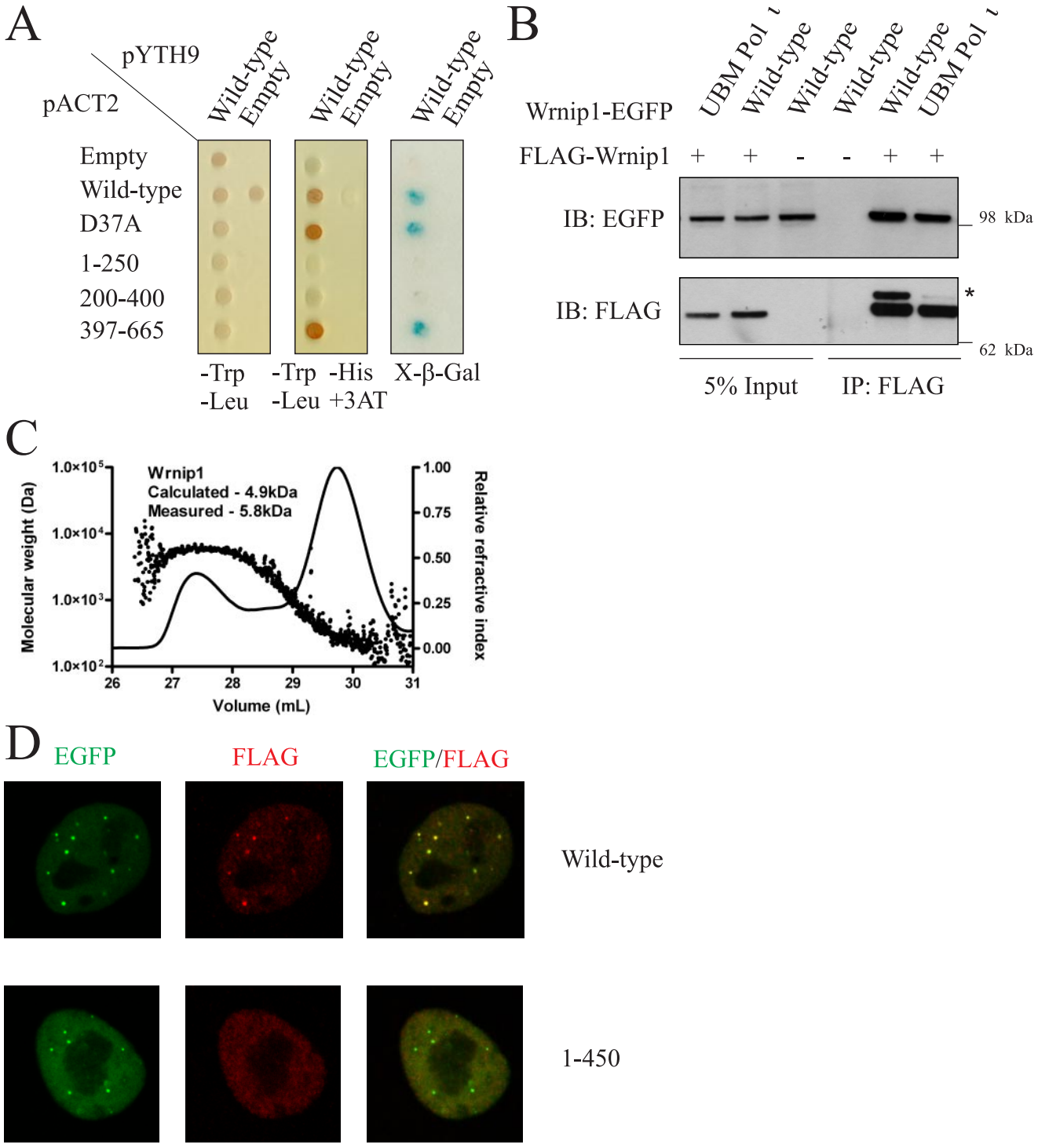

FIGURE 5. **Wrnip1 oligomerization is UBZ-independent and contributes to its presence in foci.** *A,* Ub-binding ability of Wrnip1 is not required for oligomerization. Yeast two-hybrid assay with the Y190 strain. *Empty*, control yeast transformed with the indicated empty vectors. D37A, yeast transformed with Wrnip1 D37A. *1–250*, *200–400*, *397–665*, yeast transformed with fragments of Wrnip1 encompassing amino acids from 1 to 250; from 200 to 400, and from 397 to 665, respectively. *B,* Wrnip1 UBM$^{Pol\iota}$ chimera oligomerizes with wild-type Wrnip1. HEK 293T cells were transfected with FLAG-Wrnip1 together with either Wrnip1-EGFP or Wrnip1 UBM$^{Pol\iota}$-EGFP chimera. Protein complexes were immune precipitated with an anti-FLAG antibody and visualized by SDS-PAGE and Western blot. *, mono-ubiquitylated Wrnip1. *IB,* immunoblot. *C,* Wrnip1 UBZ is a monomer in solution. MALLS using purified UBZ^{Wrnip1} cleaved from GST by thrombin. The *left peak* represents Wrnip1 UBZ, and the *right peak* is from small molecules. Calculated and measured molecular weights of UBZ^{Wrnip1} are shown. *D,* C terminus of Wrnip1 is required for its presence in foci. HeLa_Wrnip1-EGFP cells were transfected with FLAG-tagged Wrnip1 wild type or lacking the last 215 amino acids.

tude of unrelated functions (42, 43). Therefore, we can envision a scenario in which Wrnip1 acts as an ATPase chaperone within a broad set of subnuclear sites involved in different DNA transactions and not only replication.

Independently of their identity, the presence of Wrnip1 in all the described heterogeneous structures seems to be highly regulated and specifically depends on its UBZ. The UBZ domain of Wrnip1 is very similar to the one in the DNA damage-tolerance

factor Rad18, and the UBZ of both Wrnip1 and Rad18 can bind to mono-Ub with comparable affinities ($K_D \approx 40\ \mu M$). Wrnip1 and Rad18 also bind to Lys-63-type chains stronger than to mono-Ub. However, Rad18 appears to be able to discriminate between Lys-63 ($K_D \approx 20\ \mu M$) and Lys-48 chains ($K_D \approx 100\ \mu M$). This selectivity might contribute to the different distribution of Wrnip1 and Rad18 foci *in vivo* (Fig. 4*B*). Although at present the structural basis of this selectivity is unknown, we can trace parallels with the behavior of another type of UBD, the ubiquitin-associated domain (UBA). In a recent survey on more than 30 UBAs, it was shown that one group preferentially binds Lys-48-linked chains, a second group Lys-63 chains, whereas a third one can bind both types (44). Moreover, in different studies it was shown that the UBA domains of hHR23a and Mud1 bind between the two Ub moieties of a Lys-48-type di-Ub chain in a "sandwich-like" manner (45, 46), whereas the UBA domain of hHR23a binds to Lys-63-linked di-Ub chains in a similar way as it binds to mono-Ub (47, 48).

The mechanistic link between foci formation and Ub-binding ability appears to be less clear. Indeed, as previously shown for Y-family polymerases (13, 21) and more recently for Rap80 (24, 49), also in the case of Wrnip1, a Ub-binding module is necessary to be localized in nuclear foci, independently of DNA damage. However, Ub-binding ability *per se* does not suffice for Wrnip1 to be present in different subnuclear structures. A Wrnip1 $UBZ^{Pol\eta}$ chimera is not localized inside foci, despite carrying a zinc finger domain similar to the one of Wrnip1 (Fig. 4*C*). Moreover, Wrnip1 and Rad18, which carry very similar UBZ4-type domains, do not fully co-localize, even after UVC-induced DNA damage (Fig. 4*B*). Therefore, UBZ alone is likely insufficient to drive Wrnip1 to various subnuclear structures and additional binding sites may determine specificity toward certain loci. This phenomenon has been described previously for translesion polymerases η and ι, which concentrate in UV-induced foci via a dual interaction with ubiquitylated PCNA that involves both their UBD and PIP box (PCNA-interacting peptide) (13). To this respect, it is interesting that a C-terminal deletion of Wrnip1, reducing its ability to oligomerize, is already sufficient to prevent its localization inside nuclear foci (Fig. 5*D*).

In conclusion, our study reveals Wrnip1 as a new member of a growing family of UBD-containing proteins that use their specific UBDs to localize in nuclear focal structures, not only after induced DNA damage but also in unstimulated cells. Our morphological data also indirectly highlight possible functions of Wrnip1 in human cells. Beside replication, Wrnip1 ATPase could be a chaperone engaged in several transactions in the nucleus.

Acknowledgments—We thank Alan Lehmann, Helle Ulrich, and Roberto Chiarle for their critical reading of the manuscript and constructive comments. We are grateful to Pim van Dijk and Mark Luna-Vargas from the Sixma laboratory, for producing the di-Ub chains used in the SPR experiments.

REFERENCES

1. Branzei, D., and Foiani, M. (2008) *Nat. Rev. Mol. Cell Biol.* **9,** 297–308
2. Moldovan, G. L., Pfander, B., and Jentsch, S. (2007) *Cell* **129,** 665–679
3. Hishida, T., Iwasaki, H., Ohno, T., Morishita, T., and Shinagawa, H. (2001) *Proc. Natl. Acad. Sci. U. S. A.* **98,** 8283–8289
4. Hickson, I. D. (2003) *Nat. Rev. Cancer* **3,** 169–178
5. Kudlow, B. A., Kennedy, B. K., and Monnat, R. J., Jr. (2007) *Nat. Rev. Mol. Cell Biol.* **8,** 394–404
6. Crabbe, L., Jauch, A., Naeger, C. M., Holtgreve-Grez, H., and Karlseder, J. (2007) *Proc. Natl. Acad. Sci. U. S. A.* **104,** 2205–2210
7. Crabbe, L., Verdun, R. E., Haggblom, C. I., and Karlseder, J. (2004) *Science* **306,** 1951–1953
8. Hishida, T., Ohno, T., Iwasaki, H., and Shinagawa, H. (2002) *EMBO J.* **21,** 2019–2029
9. Hishida, T., Ohya, T., Kubota, Y., Kamada, Y., and Shinagawa, H. (2006) *Mol. Cell. Biol.* **26,** 5509–5517
10. Kim, J. H., Kang, Y. H., Kang, H. J., Kim, D. H., Ryu, G. H., Kang, M. J., and Seo, Y. S. (2005) *Nucleic Acids Res.* **33,** 6137–6150
11. Tsurimoto, T., Shinozaki, A., Yano, M., Seki, M., and Enomoto, T. (2005) *Genes Cells* **10,** 13–22
12. Bish, R. A., and Myers, M. P. (2007) *J. Biol. Chem.* **282,** 23184–23193
13. Bienko, M., Green, C. M., Crosetto, N., Rudolf, F., Zapart, G., Coull, B., Kannouche, P., Wider, G., Peter, M., Lehmann, A. R., Hofmann, K., and Dikic, I. (2005) *Science* **310,** 1821–1824
14. Notenboom, V., Hibbert, R. G., van Rossum-Fikkert, S. E., Olsen, J. V., Mann, M., and Sixma, T. K. (2007) *Nucleic Acids Res.* **35,** 5819–5830
15. Geiser, M., Cebe, R., Drewello, D., and Schmitz, R. (2001) *BioTechniques* **31,** 88–90, 92
16. Hecker, C. M., Rabiller, M., Haglund, K., Bayer, P., and Dikic, I. (2006) *J. Biol. Chem.* **281,** 16117–16127
17. Bomar, M. G., Pai, M. T., Tzeng, S. R., Li, S. S., and Zhou, P. (2007) *EMBO Rep.* **8,** 247–251
18. Yoshimura, A., Seki, M., Hayashi, T., Kusa, Y., Tada, S., Ishii, Y., and Enomoto, T. (2006) *Biol. Pharm. Bull.* **29,** 2192–2196
19. Hayashi, T., Seki, M., Inoue, E., Yoshimura, A., Kusa, Y., Tada, S., and Enomoto, T. (2008) *Genes Genet. Syst.* **83,** 95–100
20. Nakajima, S., Lan, L., Kanno, S., Usami, N., Kobayashi, K., Mori, M., Shiomi, T., and Yasui, A. (2006) *J. Biol. Chem.* **281,** 34687–34695
21. Guo, C., Tang, T. S., Bienko, M., Parker, J. L., Bielen, A. B., Sonoda, E., Takeda, S., Ulrich, H. D., Dikic, I., and Friedberg, E. C. (2006) *Mol. Cell. Biol.* **26,** 8892–8900
22. Kim, H., Chen, J., and Yu, X. (2007) *Science* **316,** 1202–1205
23. Kim, H., Huang, J., and Chen, J. (2007) *Nat. Struct. Mol. Biol.* **14,** 710–715
24. Liu, Z., Wu, J., and Yu, X. (2007) *Nat. Struct. Mol. Biol.* **14,** 716–720
25. Hicke, L., Schubert, H. L., and Hill, C. P. (2005) *Nat. Rev. Mol. Cell Biol.* **6,** 610–621
26. Hurley, J. H., Lee, S., and Prag, G. (2006) *Biochem. J.* **399,** 361–372
27. Li, B., and de Lange, T. (2003) *Mol. Biol. Cell* **14,** 5060–5068
28. Pageau, G. J., and Lawrence, J. B. (2006) *J. Cell Biol.* **175,** 693–701
29. Cremer, T., Cremer, M., Dietzel, S., Muller, S., Solovei, I., and Fakan, S. (2006) *Curr. Opin. Cell Biol.* **18,** 307–316
30. Yuasa, M. S., Masutani, C., Hirano, A., Cohn, M. A., Yamaizumi, M., Nakatani, Y., and Hanaoka, F. (2006) *Genes Cells* **11,** 731–744
31. Cioce, M., and Lamond, A. I. (2005) *Annu. Rev. Cell Dev. Biol.* **21,** 105–131
32. Pohl, C., and Jentsch, S. (2008) *Cell* **132,** 832–845
33. Watanabe, K., Tateishi, S., Kawasuji, M., Tsurimoto, T., Inoue, H., and Yamaizumi, M. (2004) *EMBO J.* **23,** 3886–3896
34. Kawabe, Y., Seki, M., Yoshimura, A., Nishino, K., Hayashi, T., Takeuchi, T., Iguchi, S., Kusa, Y., Ohtsuki, M., Tsuyama, T., Imamura, O., Matsumoto, T., Furuichi, Y., Tada, S., and Enomoto, T. (2006) *DNA Repair* **5,** 816–828
35. Ulrich, H. D., and Jentsch, S. (2000) *EMBO J.* **19,** 3388–3397
36. Miyase, S., Tateishi, S., Watanabe, K., Tomita, K., Suzuki, K., Inoue, H., and Yamaizumi, M. (2005) *J. Biol. Chem.* **280,** 515–524
37. Kawabe, Y., Branzei, D., Hayashi, T., Suzuki, H., Masuko, T., Onoda, F., Heo, S. J., Ikeda, H., Shimamoto, A., Furuichi, Y., Seki, M., and Enomoto, T. (2001) *J. Biol. Chem.* **276,** 20364–20369
38. Gray, M. D., Wang, L., Youssoufian, H., Martin, G. M., and Oshima, J. (1998) *Exp. Cell Res.* **242,** 487–494
39. Suzuki, T., Shiratori, M., Furuichi, Y., and Matsumoto, T. (2001) *Oncogene* **20,** 2551–2558

40. von Kobbe, C., and Bohr, V. A. (2002) *J. Cell Sci.* **115,** 3901–3907
41. Bernardi, R., and Pandolfi, P. P. (2007) *Nat. Rev. Mol. Cell Biol.* **8,** 1006–1016
42. Tucker, P. A., and Sallai, L. (2007) *Curr. Opin. Struct. Biol.* **17,** 641–652
43. Wang, Q., Song, C., and Li, C. C. (2004) *J. Struct. Biol.* **146,** 44–57
44. Raasi, S., Varadan, R., Fushman, D., and Pickart, C. M. (2005) *Nat. Struct. Mol. Biol.* **12,** 708–714
45. Trempe, J. F., Brown, N. R., Lowe, E. D., Gordon, C., Campbell, I. D., Noble, M. E., and Endicott, J. A. (2005) *EMBO J.* **24,** 3178–3189
46. Varadan, R., Assfalg, M., Raasi, S., Pickart, C., and Fushman, D. (2005) *Mol. Cell* **18,** 687–698
47. Varadan, R., Assfalg, M., Haririnia, A., Raasi, S., Pickart, C., and Fushman, D. (2004) *J. Biol. Chem.* **279,** 7055–7063
48. Ikeda, F., and Dikic, I. (2008) *EMBO Rep.* **9,** 536–542
49. Sobhian, B., Shao, G., Lilli, D. R., Culhane, A. C., Moreau, L. A., Xia, B., Livingston, D. M., and Greenberg, R. A. (2007) *Science* **316,** 1198–1202

Human Wrnip1 Is Localized in Replication Factories in a Ubiquitin-binding Zinc Finger-dependent Manner

Nicola Crosetto, Marzena Bienko, Richard G. Hibbert, Tina Perica, Chiara Ambrogio, Tobias Kensche, Kay Hofmann, Titia K. Sixma and Ivan Dikic

J. Biol. Chem. 2008, 283:35173-35185.
doi: 10.1074/jbc.M803219200 originally published online October 7, 2008
